# Optimal non-uniform fast Fourier transform for high-speed swept source optical coherence tomography

**Tong Wu (吴 彤)* and Youwen Liu (刘友文)**

*College of Science, Nanjing University of Aeronautics and Astronautics, Nanjing 210016, China*

**Corresponding author: wutong@nuaa.edu.cn*

Received August 17, 2012; accepted October 10, 2012; posted online January 21, 2013

Convolution kernel-based non-uniform fast Fourier transform (NUFFT) is an effective image reconstruction method for Fourier domain optical coherence tomography. By measuring the reconstruction error, a general method for finding the optimal parameters of the kernel function is investigated. Performances in terms of point spread function and computation time are evaluated. The NUFFT with optimal parameters yields signal sensitivity of over 40 dB, with a computation time that is decreased by 85% compared with the conventional oversampling NUFFT. *In vivo* images of finger tissue are efficiently reconstructed through the proposed reconstruction method.

*OCIS codes:* 170.4500, 060.2350.

*doi: 10.3788/COL201311.021702.*

Optical coherence tomography (OCT) is a high-resolution biomedical imaging technique, which is capable of non-invasive imaging of highly scattered biological tissue[1]. Fourier domain OCT (FD-OCT) has attracted considerable attention due to the great improvements in axial-scan (A-scan) rate and detection sensitivity over time domain OCT (TD-OCT)[2]. Two implementations of FD-OCT are the spectral domain OCT (SD-OCT) and swept source OCT (SS-OCT). For FD-OCT, high quality images can be reconstructed efficiently by fast Fourier transform (FFT) if the spectral interference signal is sampled with uniform intervals in the wavenumber ($k$) domain. Unfortunately, the signal is not commonly recorded as that case. In a typical SD-OCT system, the spectral components of the interference signal are dispersed linearly in wavelength ($\lambda$) by a diffraction grating. The non-linear relationship between $\lambda$ and $k$ (i.e., $k = 2\pi/\lambda$) causes the captured spectral interference data to be unevenly distributed in the $k$ domain. For the majority case of the SS-OCT system, the spectral interference signal is unevenly sampled in the $k$ domain, because the $k$ versus time ($t$) relationship is commonly nonlinear due to the general tuning mechanism of a swept source. Direct FFT of this nonlinear-in-$k$ data introduces significant reconstruction errors that dramatically compromise the performance of FD-OCT system in terms of axial resolution and signal to noise ratio (SNR)[3].

Various approaches have been proposed to resolve the non linear-in-$k$ issue. Both the custom designed linear-in-$k$ spectrometer[4] for SD-OCT and $k$-linear swept source[5] for SS-OCT have been successfully implemented; however, they are not commonly used due to the delicate hardware design and increased system complexity. Another hardware-based solution for SS-OCT relies on the external $k$-trigger devices[6], which also increase the total cost of the system, making them inappropriate for the SD-OCT system. Signal processing approaches are popularly applied in both SD-OCT and SS-OCT systems due to their flexibility and interchangeability. Provided with the relationship of $k$ versus $t$ or $\lambda$ versus pixel, the spectral interference signal at uniform $k$ grids can be re-sampled by various interpolation algorithms. Linear interpolation[3], zero-filling interpolation[7], and cubic spline interpolation in the time[8] and $k$ domains[9] have been implemented in both branches of FD-OCT. Of these, linear interpolation is actually the fastest technique. However, due to the large interpolation error, linear interpolation method produces inaccurate reconstruction results, especially at the deep imaging depth. In comparison, the spline interpolation algorithm can produce results more accurately but the computation speed is still not satisfied.

Non-uniform discrete Fourier transform (NDFT) algorithm is first implemented in FD-OCT by direct multiplication of the raw-sampled nonlinear-in-$k$ data and a Vandermonde matrix[10]. Although the NDFT algorithm provides the most exact reconstruction result, the slow computation speed hinders its real-time application. Non-uniform FFT (NUFFT) is an approximation of the NDFT algorithm with much faster processing speed[11], and has been recently implemented in FD-OCT. Kaiser-Bessel (KB) kernel[12,13] and Gaussian kernel[14,15] have been independently used as the convolution kernel function for NUFFT. The selection of convolution kernel function is investigated by Chan *et al.*, and the Gaussian kernel function is considered to be a better choice for on-the-fly data processing[15]. However, the re-sampling ratio for the Gaussian kernel is limited to at least two, similar to the traditional gridding method used in magnetic resonant imaging (MRI). In theory, significant improvements in computation speed can be achieved while maintaining high accuracy by non-oversampling NUFFT. Therefore, the two important parameters, namely, re-sampling ratio and kernel width, should be optimized in order to reduce computation time further. For large scale data processing, the required memory can also be reduced with appropriately chosen parameters.

In this letter, the Gaussian kernel-based NUFFT with the optimal parameters (i.e., optimal NUFFT) is investigated. A general approach for choosing the optimal parameters is presented. For optimal NUFFT, the selected parameters of the convolution kernel are implemented for high accuracy signal reconstruction with reduced computation time. Performances in terms of point spread func-

 

tion (PSF) and computation time of various reconstruction methods are evaluated and compared. We employ the proposed optimal NUFFT method in efficiently reconstructing in vivo human finger tissue image so as to demonstrate its practical performance.

In SS-OCT, the raw spectral interference data are obtained directly by a data acquisition (DAQ) card, and can be expressed in $k$ space as

$$I(k_n) = \sum_m \sqrt{R_{\rm ref} R_{\rm s}(z_m)} \cdot S(k_n) \cdot \cos(k_n \cdot z_m), \quad n = 1, \cdots N-1, \tag{1}$$

where $R_{\rm ref}$ and $R_{\rm s}(z_m)$ represent the reflectivity of the reference mirror and the imaged sample, respectively; $z_m$ represents the optical path difference (OPD) between the sample and reference arm; $k_n$ is the wavenumber corresponding to the $n$th data of the total $N$ data; $S(k_n)$ is the power spectral density of the swept source.

Various reconstruction methods require an accurate calibration procedure for the swept source due to the nonlinear-in-$k$ issue. Thus, the wavenumber is regarded as an a priori known value for all time sampling data points. The reconstruction methods considered below are optimal NUFFT, conventional oversampling NUFFT, NDFT, and spectral phase based $k$ domain spline interpolation (KDSI).

The NUFFT is extensively investigated in a MRI field for $k$-domain mapping, and is termed as the "gridding" method. The basic NUFFT algorithm (Fig. 1) consists of several steps listed below.

1) convolving the nonlinear-in-$k$ spectral interference data with a convolution kernel;

2) re-sampling the result on a series of linear-in-$k$ locations;

3) performing a FFT on the re-sampled data;

4) dividing by the Fourier transform of the convolution kernel function.

With these steps, the NUFFT algorithm can be expressed as

$$i_{\rm NUFFT}(m) = {\rm FFT}\left\{\sum_{n=0}^{N-1} I(k_n) \cdot C(k_m - k_n)\right\} \cdot \frac{1}{c(m)}, \tag{2}$$

where $C(k)$ represents the convolution kernel function in $k$ space, and $c(z)$ represents the Fourier transform of

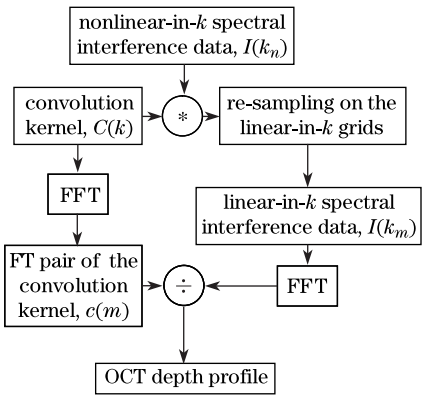


Fig. 1. OCT signal processing flow chart using NUFFT.

$C(k)$. The variable $m$ represents the depth measure proportional to $z$. The term $\sum_{n=0}^{N-1} I(k_n) \cdot C(k_m - k_n)$ represents the convolution and re-sampling steps. The re-sampling grids $k_m$ are determined by the wavenumber range ($k_{\rm max}$ to $k_{\rm min}$), total data number $N$ and the re-sampling ratio $\alpha$, and is expressed as

$$k_m = m \cdot \frac{k_{\rm max} - k_{\rm min}}{\alpha N}, \quad k_n \in [k_{\rm min}, k_{\rm max}], \quad m = 1, \cdots \alpha N. \tag{3}$$

Given the fast fall-off characteristics of the convolution kernel function, only a finite number of points have effective values for reconstruction, whose total number is defined as the effective width of the kernel. According to the effective width, a square window function is multiplied to the kernel function. Only the data within the effective kernel width must be calculated for convolution, and the data outside of the effective width are directly set to zero, as shown in

$$C(k_m - k_n) = \begin{cases} \exp\left[-\dfrac{(k_n - k_m)^2}{(\delta k)^2 \cdot 4\tau}\right], & \dfrac{|k_n - k_m|}{\delta k} < \dfrac{W}{2} \\ 0, & \text{else} \end{cases}, \tag{4}$$

where $\tau$ represents a shape parameter relative to the re-sampling ratio $\alpha$ and kernel width $W$, and $\delta k$ represents the constant wavenumber interval between each re-sampling grid. To optimize the reconstruction accuracy, the equation for the optimal value of $\tau$ is given as[11]

$$\tau = \frac{W \cdot \pi}{N^2 \cdot 2 \cdot \alpha \cdot (\alpha - 0.5)}. \tag{5}$$

NUFFT is considered as the approximation of the exact NDFT algorithm. Thus, the intrinsic reconstruction error by the NUFFT algorithm is defined as

$$E(m) = |i_{\rm NUFFT}(m) - i_{\rm NDFT}(m)|, \tag{6}$$

where $i_{\rm NDFT}(m)$ and $i_{\rm NUFFT}(m)$ are the reconstructed axial profiles by NDFT and NUFFT, respectively, and $m$ represents the depth measurement.

The evaluated reconstruction error function expressed in dB is given as

$$\varepsilon = \frac{1}{\alpha N} \sum_m |20{\rm lg}\,[i_{\rm NUFFT}(m)] - 20{\rm lg}\,[i_{\rm NDFT}(m)]|. \tag{7}$$

The reconstruction error is determined by the Fourier transform of convolution kernel, which is dependent on the kernel width $W$ and the re-sampling ratio $\alpha$.

Computation speed, another key performance, is largely dependent on the computational complexity of the reconstruction algorithm. The computational complexity of the convolution kernel-based NUFFT is proportional to $O[cWN + \alpha N{\rm lg}(\alpha N)]$, where $c$ represents a constant determined by the complexity of the convolution kernel, and $N$ is the total number of the raw data before re-sampling. Thus, in reconstructing the signal as fast as possible, the re-sampling ratio $\alpha$ and the kernel width $W$ must be set as small as possible.

In this letter, the optimal parameters were identified

by evaluating the reconstruction error. The A-scan signal was processed under an initial value of $\alpha$ and $W$ , after which the reconstruction error was calculated according to Eq. (7). Each reconstruction error was added into an error array. By slightly tuning the value of the parameters until all the parameters considered were tested, all of the reconstruction error corresponding to the different parameters were calculated. Then the reconstruction errors array under different values of re-sampling ratio $\alpha$ and kernel width $W$ were obtained. Given an acceptable reconstruction error threshold, the optimal parameters were selected, which also ensured the total data number after re-sampling be a power of two.

In order to compare the reconstruction performances of the optimal NUFFT method, two other reconstruction methods were implemented for the same A-scan data, including NDFT algorithm and KDSI algorithm.

The definition of the NDFT of the raw-sampled A-scan signal $I(k_n)$ is given as[10−15]

$$\begin{aligned} & i_{\mathrm{NDFT}}(m) \\ &= \sum_{n=1}^{N} I(k_n) \cdot \exp\left[-\mathrm{j} \cdot \frac{2\pi}{k_{\max} - k_{\min}} \cdot (k_n - k_{\min}) \cdot m\right], \\ & m = n = 1, \cdots, N. \end{aligned} \tag{8}$$

The symbol used in Eq. (8) is the same as that in Eqs. (2) and (3). Usually Eq. (8) is expressed in the form of matrix multiplication as follows: $i = \mathbf{D} \cdot I$, where

$$\mathbf{D} = \begin{bmatrix} 1 & 1 & \cdots & 1 \\ p_0^1 & p_1^1 & \cdots & p_{N-1}^1 \\ \vdots & \vdots & \cdots & \vdots \\ p_0^{N-1} & p_1^{N-1} & \cdots & p_{N-1}^{N-1} \end{bmatrix}, \tag{9}$$

and $p = \exp\left[-\mathrm{j} \cdot \frac{2\pi}{k_{\max} - k_{\min}} \cdot (k_n - k_{\min})\right]$.

The computation of NDFT involves $O[N^2]$ operations. Compared with the computational complexity of NUFFT, the NDFT method is redundant and is not practical for real-time imaging.

Meanwhile, the KDSI method has been proposed for SS-OCT image reconstruction with high efficiency[9]. After the Hilbert transform of a calibration-used Mach-Zehnder interferometer (MZI) signal, the resulting complex MZI calibration signal is given as

$$\hat{I}_{\mathrm{MZI}}[t_n] = 2S(t_n) \cdot R \cdot \exp(j \cdot \phi[t_n]) \quad n = 1, \cdots, N, \tag{10}$$

where $R$ represents a scale factor, $d$ is the OPD between the two arms in the MZI, $t_n$ is the time instant of the $n$-th data point, and $S(t_n)$ is the spectral envelope of the swept source. Hence, the $N$-point $k$-uniform grids are obtained from the unwrapped spectral phase of this complex MZI calibration signal, and are given as

$$k[m] = m \cdot \frac{\phi[t_{N-1}] - \phi[t_1]}{\alpha \cdot N \cdot d} = m \cdot \frac{k[t_N]}{\alpha \cdot N}, \quad m = 1, \cdots, \alpha N, \tag{11}$$

where $\alpha$ represents the re-sampling ratio. Based on the Eq. (11), the $N$-point linear-in-$k$ OCT imaging signal can be obtained according to the $\alpha N$-point linear-in-$k$ grids by linear or spline interpolation.

Using the spline function of order $m$ to interpolate the $\alpha N$-points data involves a computational complexity of $O[m^2 \alpha N]$. Then, the KDSI-based data processing involves the FFT of the $\alpha N$-points linear-in-$k$ data. Therefore, the total computational complexity of KDSI-based OCT image reconstruction is $O[m^2 \alpha N + \alpha N \lg(\alpha N)]$.

The custom-designed high-speed SS-OCT system used in this study has been previously described in detail[9]. The swept laser source covers a wavelength sweeping range of 110 nm, which is centered around 1310 nm. The SS-OCT imaging system was configured as a balanced detection type Michelson interferometer. Of these, 90% of the output power of the swept source was fed into the imaging interferometer through a wideband circulator. The sample beam was scanned by an X-Y galvo-mirror scanner, and then focused by an achromatic doublet with the focal length of 60 mm. The lateral resolution was 12 $\mu$m according to the optics used in the sample arm. The OCT signal was detected by the balanced photon detector and sampled by a high-speed DAQ card. To overcome the non-repeatability and non-stable effect of the commercial swept source, an MZI was added into the system for real-time calibration. The MZI spectral interference signal was sampled by another analog input port of the DAQ card.

In order to identify the optimal parameters, a simulated noise-free spectral interference signal was used to calculate the reconstruction error. The spectral interference signal corresponding to a three-layered sample was simulated to evaluate the signal composite reconstruction performance from the superficial and deep locations of the sample. Considering the practical light penetration depth in biological tissue, depths of 2.5, 3.5, and 4.5 mm were chosen for determining the optimal parameters. The re-sampling ratio was set to the 40 values evenly distributed between 0.5 and 2, and the width parameter $W$ was set to the 40 values evenly distributed between 0.01 and 6. By slightly tuning the values of re-sampling ratio $\alpha$ and kernel width $W$, 1600 reconstruction error values were obtained for the reconstruction error array. The red curve represents the simulated PSF signal reconstructed by the NDFT algorithm, and the blue curve is by the conventional oversampling NUFFT algorithm (Fig. 2(a)). The oversampling ratio was set to 2, and the convolution kernel width $W$ was set to 6. The reconstructed PSF by NUFFT algorithm is close to that by the NDFT, thereby confirming the fidelity of the custom-developed NUFFT algorithm. The values of the color correspond to the reconstruction error values; in addition, the conventional parameter pair of $\alpha = 2$ and $W = 6$ has a small error value (Fig. 2(b)). However, for the smaller re-sampling ratio $\alpha$, the reconstruction error could also be decreased by choosing an appropriate value of $W$. Especially when $\alpha$ is set to be around 1, the reconstruction error can be maintained at a low value in a zone around the width parameter of 2. The reconstruction error can be relatively low at a narrow zone by further decreasing the re-sampling ratio, although it would still gradually worsen. Theoretically, the NUFFT with optimal parameters improve the computation speed and ensure a high quality reconstruction of SS-OCT signal. This assumption is confirmed through the reconstruction

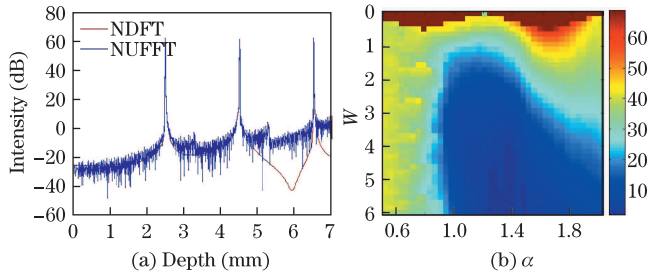


Fig. 2. (Color online) Simulated PSF comparison and reconstruction error arrays obtained by slightly tuning the (a) re-sampling ratio $\alpha$ and (b) convolution kernel width $W$.

of biological tissue images in the following section.

The sampling rate of DAQ was set to 50 MS/s, so that 2048 data points could be obtained for each A-scan. Due to the duty cycle of the swept source, the raw-sampled non-linear-in-$k$ data for each A-scan consisted of 1941 data points. For efficient FFT computation of the linear-in-$k$ data, 2048 or 4096 points should be generated. Then, the corresponding re-sampling ratios should be 1.055, and 2.11, respectively. The kernel width of the Gaussian convolution kernel is optimized by the proposed parameter finding method in the previous section. Corresponding to the re-sampling ratio $\alpha$ of 1.055, kernel width W was set to be 2.25. For the conventional NUFFT, the parameters of $\alpha = 2.11$ and $W = 6$ were used. The results of PSFs with OPD of 3.2 mm reconstructed under the two parameter pairs are shown in Fig. 3(a). The PSF reconstructed by NDFT, represented as the blue dots, is free from artifacts and has a low noise level. The PSFs in red dots and green solid lines are obtained from NUFFT with re-sampling ratios of 2.11 and 1.055, respectively. The reconstructed PSFs are identical with that from NDFT. However, for the conventional oversampling case, oversampling with $\alpha N$ points introduces the appearance of identical copies of the spectrum as some levels of aliasing artifact at every $\alpha N$ frequency interval in the $z$ domain for the FD-OCT signal. Therefore, extra data points of the reconstructed depth profile due to oversampling were truncated to prevent the aliasing artifacts into the imaging range[11]. Figure 3(b) shows the practical used Gaussian convolution kernels at an arbitrary wavenumber position corresponding to the optimal and conventional cases. The effective numbers of points used in the convolution kernel were 3 and 12, respectively. According to the reconstruction error equation, for the oversampling NUFFT case, the reconstruction error is 5.51, and the error for the optimal NUFFT case is 5.67. Meanwhile, the number of data points for FFT is decreased to 2048 points from the oversampling case, where 4096 points are processed. Therefore, a comparable reconstruction result is maintained with less computation required.

In order to evaluate the performance of the presented optimal NUFFT method in the comparison of the NDFT and KDSI methods, the spectral interference signal corresponding to several depths was measured with a reflective mirror as the sample. The PSFs reconstructed from the optimal NUFFT, KDSI and NDFT methods are shown in the Figs. 4(a), (b) and (c), respectively. Each graph presents the PSFs measured at positions ranging from 0.1 mm to 4 mm relative to the zero optical path length difference. The result reconstructed by the proposed optimal NUFFT method provides the accurate signal compared with those by the NDFT method. For clear comparison, the intensity of the PSF decreasing curve, often called the sensitivity fall-off curve, is depicted in Fig. 4(d). We can see that the optimal NUFFT method provides sensitivity, which is close to that by NDFT method, but the KDSI method provides the relatively lower sensitivity signal, especially at the large depths. The different performances of the three methods for the large depths possibly result from the relatively large interpolation error during the process of convolution or spline interpolation to the high frequency spectral interference signal. The convolution-based method results in relatively small error compared with spline interpolation. The SNR of the SS-OCT system at the effective imaging range is also experimentally confirmed to be higher than 40 dB (Fig. 4(a)).

In order to evaluate and compare the computation speed of the optimal NUFFT method with the conventional oversampling NUFFT, NDFT and KDSI methods, the spectral interference signal was post-processed using these reconstruction methods. The processing times were measured by a custom-designed MATLAB® program. Table 1 presents the computation time of the different methods. The program was run on a computer with an

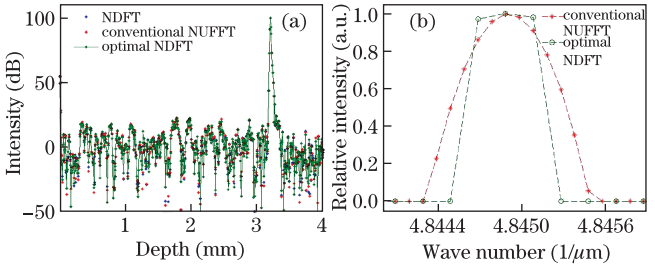


Fig. 3. (Color online) (a) PSF reconstructed by NDFT, conventional oversampling, and optimal NUFFT, and (b) their corresponding convolution kernels.

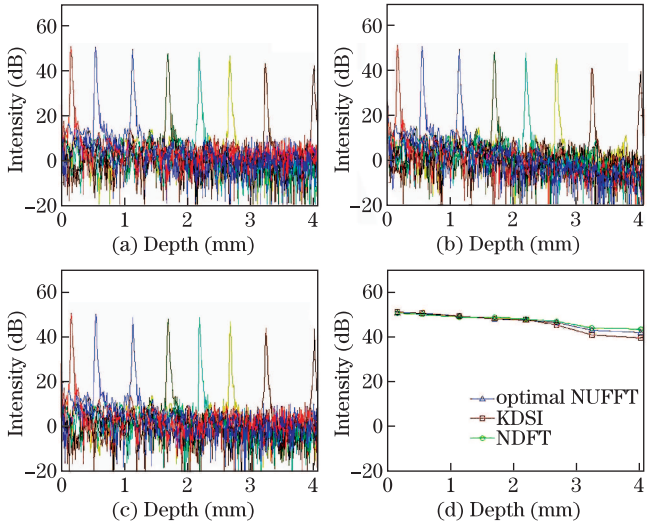


Fig. 4. (Color online) PSFs reconstructed from the optimal (a) NUFFT, (b) KDSI, and (c) NDFT methods, and (d) their respective sensitivity fall-off curves.

**Table 1. Computation Time ($\mu$s) for Each 1941-Point A-Scan from Various Reconstruction Methods**

| Method | Oversampling Ratio $\alpha$ | | |
|---|---|---|---|
| | 1 | 1.055 | 2.11 |
| NDFT | 1039 | | |
| NUFFT | $W = 2.25$ | 6.59 | |
| | $W = 6$ | 22.1 | 42.7 |
| KDSI | 119 | | |

Intel Core i5 processor (2.53 GHz) and 2 GB RAM. The data processing was realized on a single thread computing, but further enhancement of computation efficiency can be achieved through parallel computing by employing multi-thread processing.

Due to the computation complexity of $O[N^2]$ of the NDFT method, the measured computation time for the case of NDFT is 1-order of magnitude larger than that of the KDSI method and 2-order larger than that of the NUFFT methods, thus confirming the impracticality of NDFT for real-time OCT reconstruction. The KDSI method is a faster approach compared with the NDFT method. However, signal inaccuracy due to the spline interpolation decreases the reconstruction accuracy, and the computation speed is still slower than NUFFT based methods. The computation time for one 1941-point A-Scan by the optimal NUFFT with $\alpha = 1.055$ and $W = 2.25$ is 6.59 $\mu$s (Table 1). In contrast, the conventional oversampling NUFFT with $\alpha = 2.11$ and $W = 6$ needed 42.7 $\mu$s to process the same raw data. This indicates that the computation time of the proposed method is reduced by 85% compared with the conventional oversampling NUFFT method. Meanwhile, the data storage space needed for the optimal NUFFT method is less than that of the other methods, which is advantageous when a large scale data set is processed with high computation speed.

The performance of the optimal NUFFT method is further evaluated for in vivo SS-OCT image reconstruction. The reconstructed OCT image of human fingernail fold tissue is presented in Fig. 5, where (a), (b) and (c) correspond to the images reconstructed by the NDFT and the optimal NUFFT and KDSI methods, respectively. For the optimal NUFFT method, 2048 re-sampled data points corresponding to the re-sampling ratio $\alpha$ of 1.055 and convolution kernel width $W$ of 2.25 were processed. The image was converted to logarithm scale before mapping to gray scale value. The image clearly shows the tissue structures, such as epidermis (E), cuticle (C), nail plate (NP), nail bed (NB), and dermis (D). Very good results are obtained by the optimal NUFFT, which shows comparable image quality with that by NDFT. As shown in the two red square boxes in Figs. 5(b) and (c), the optimal NUFFT offers superior sensitivity performance compared with the KDSI method, especially at a large depth. This is in agreement with the results of the PSF. Furthermore, the optimal NUFFT has much faster computation speed, which optimizes the trade-off between image quality and computation time.

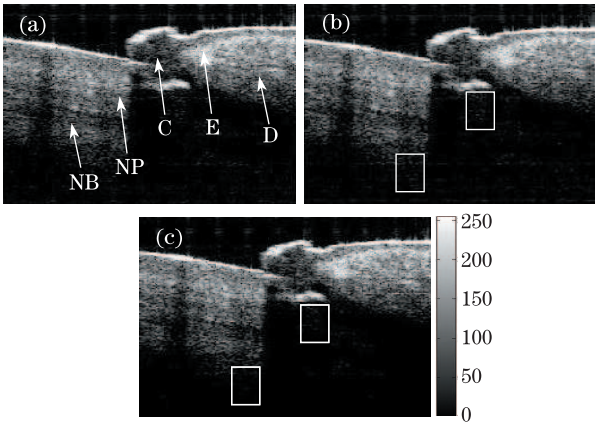


Fig. 5. (Color online) SS-OCT images of human fingernail fold reconstructed by (a) NDFT, (b) optimal NUFFT, and (c) KDSI methods.

An optimal NUFFT method with Gaussian convolution kernel is evaluated for fast and accurate FD-OCT image reconstruction. A general kernel parameter finding method is introduced. For an optimized convolution kernel function, the parameters are finely tuned and chosen to allow an acceptable level of low reconstruction error. The performance advantage of the proposed optimal NUFFT is experimentally confirmed by evaluating the PSFs obtained from a custom-built SS-OCT system. Several typical methods, including the NDFT, KDSI, and the conventional oversampling NUFFT methods are implemented for performance comparison. The optimal NUFFT with a re-sampling ratio $\alpha$ of 1.055 and kernel width $W$ of 2.25 provides good results with the computation time decreased by 85%. Finally, in vivo image reconstructed with high quality is demonstrated by the reconstruction methods, which thus confirming the feasibility of the proposed method.

We acknowledge Prof. Zhihua Ding for sharing the OCT image data of human fingernail fold. This work was supported by the National Natural Science Foundation of China (Nos. 61205201 and 11174147), the Fundamental Research Funds for the Central Universities, Nanjing University of Aeronautics and Astronautics (No. NZ2012305), the Nanjing University of Aeronautics and Astronautics Scientific Research Fund for Person with Ability in Draught (No. 56YAH12011), and the Postdoctoral Research Funds of Jiangsu Province (No. 1201034C).

## References

1. D. Huang, E. A. Swanson, C. P. Lin, J. S. Schuman, W. G. Stinson, W. Chang, M. R. Hee, T. Flotte, K. Gregory, C. A. Puliafito, and J. G. Fujimoto, Science **254,** 1178 (1991).
2. J. F. de Boer, B. Cense, B. H. Park, M. C. Pierce, G. J. Tearney, and B. E. Bouma, Opt. Lett. **28,** 2067 (2003).
3. S. Yun, G. Tearney, J. de Boer, N. Iftimia, and B. Bouma, Opt. Express **11,** 2953 (2003).
4. Z. Hu and A. M. Rollins, Opt. Lett. **32,** 3525 (2007).
5. C. M. Eigenwillig, B. R. Biedermann, G. Palte, and R. Huber, Opt. Express **16,** 8916 (2008).
6. J. Zhang, J. S. Nelson, and Z. Chen, Opt. Lett. **30,** 147

(2005).

7. Y. Yasuno, V. D. Madjarova, S. Makita, M. Akiba, A. Morosawa, C. Chong, T. Sakai, K.-P. Chan, M. Itoh, and T. Yatagai, Opt. Express **13,** 10652 (2005).
8. E. Götzinger, M. Pircher, R. A. Leitgeb, and C. K. Hitzenberger, Opt. Express **13,** 583 (2005).
9. T. Wu, Z. H. Ding, L. Wang, and M. H. Chen, Opt. Express **19,** 18430 (2011).
10. T. Wu, Z. H. Ding, K. Wang, and C. Wang, Chin. Opt. Lett. **7,** 941 (2009).
11. K. K. H. Chan and S. Tang, Biomed. Opt. Express **1,** 1309 (2010).
12. D. Hillmann, G. Huttmann, and P. Koch, Proc. SPIE **7372,** 73720R (2009).
13. S. Vergnole, D. Lévesque, and G. Lamouche, Opt. Express **18,** 10446 (2010).
14. K. Zhang and J. U. Kang, Opt. Express **18,** 23472 (2010).
15. K. K. H. Chan and S. Tang, Opt. Express **19,** 26891 (2011).